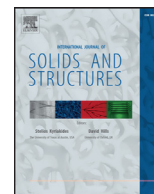




ELSEVIER

Contents lists available at ScienceDirect

International Journal of Solids and Structures

journal homepage: www.elsevier.com/locate/ijsolstr

A multiaxial load-induced thermal strain constitutive model for concrete

Giacomo Torelli^{a,*}, Martin Gillie^a, Parthasarathi Mandal^a, Van-Xuan Tran^b

^aSchool of Mechanical, Aerospace and Civil Engineering, The University of Manchester, Manchester M13 9PL, UK

^bEDF Energy, R&D UK Centre, SW1×7EN, 40 Grosvenor Place, London, UK

ARTICLE INFO

Article history:

Received 21 July 2016

Revised 12 October 2016

Available online xxx

Keywords:

Concrete

Temperature

Fire

Load-induced thermal strain

Transient thermal creep

Thermal strain

Stress confinement

Modeling

ABSTRACT

The paper presents a novel thermomechanical 3D Load-Induced Thermal Strain (LITS) model that captures the experimentally demonstrated behavior of concrete in the case of heating under multiaxial mechanical load, for temperatures up to 250 °C. In contrast to the models available in the literature, the new model takes into account the observed dependency of LITS on stress confinement. Such a dependency is introduced through a confinement coefficient which makes LITS directly proportional to the confinement of the stress state. Also, a new practical bilinear LITS model is proposed and proved to be suitable for fitting the general trend of the curves experimentally obtained for different loading conditions. The presented model is embedded in a thermoelastic material constitutive law, and then verified and validated against experiments performed on concrete specimens subjected to transient temperatures up to 250 °C under uniaxial, biaxial and triaxial compressive stress states. Once calibrated and validated, the constitutive model is used to evaluate the effects of LITS on the structural behavior of a Prestressed Concrete Pressure Vessel (PCPV) of a typical Advanced Gas cooled Reactor (AGR) subjected to a heating-cooling cycle simulating a temporary fault in its cooling system. The results of this study indicate that the development of LITS significantly influences the stress redistribution in the structure. Moreover, it is shown that in the case of PCPVs (and by extension similar structures) it is crucial to consider the LITS dependence on the stress confinement.

© 2016 The Authors. Published by Elsevier Ltd.

This is an open access article under the CC BY license (<http://creativecommons.org/licenses/by/4.0/>).

1. Introduction

Load induced thermal strain, or LITS, is a strain component that develops when concrete is heated while subjected to compressive stress states. Several studies have demonstrated that accurate and robust modeling of this strain component is crucial for reliably assessing the effects of heating-cooling cycles on concrete structures (Law and Gillie, 2008; De Borst and Peeters, 1989; Anderberg and Thelandersson, 1976; Schneider, 1976). Most of the available experimental and theoretical works focus on the development of LITS for uniaxial compressive stress states, providing a good basis for assessing the behavior of concrete framed structures, such as typical offices. However, little attention has been paid to the development of LITS in bulk concrete structures where the stress state is expected to be multiaxial, such as Prestressed Concrete Pressure Vessels (PCPV) of nuclear reactors, tunnels and vaults. With this in mind, the present paper presents a novel and robust 3D LITS material

model which overcomes some of the shortcomings of the models available in the literature.

When heated in the absence of mechanical load, concrete exhibits a volumetric thermal strain usually referred to as Free Thermal Strain (FTS). Such strain is generally expansive and is due to the interaction of different phenomena affecting the structure of the material, such as shrinkage of the cement paste and thermal expansion of the aggregates. Experimental evidence shows that if heated concrete is subjected to uniaxial compressive stress, a smaller thermal strain occurs in the direction of the load than in the case of free thermal expansion. It is this additional thermal strain component, which is defined as LITS. In other words, LITS may be seen as the difference between the thermal strains developing in the cases of concrete subjected to constant compressive stress and stress-free concrete.

According to this definition, LITS includes several strain components which are due to the development of various coupled mechanisms on heating under compressive load. Specifically, LITS includes an increment in elastic deformation due to the degradation of the elastic modulus with increasing temperature, basic and drying creep strains which develop on heating and an additional strain

* Corresponding author.

E-mail address: giacomo.torelli@manchester.ac.uk (G. Torelli).

<http://dx.doi.org/10.1016/j.ijsolstr.2016.11.017>

0020-7683/© 2016 The Authors. Published by Elsevier Ltd. This is an open access article under the CC BY license (<http://creativecommons.org/licenses/by/4.0/>).

component usually referred to as Transient Thermal Creep (TTC) (Gross, 1975; Anderberg and Thelandersson, 1976; Hager, 2013; Schneider, 1988; Khoury et al., 1985). TTC is the biggest component of LITS (Anderberg and Thelandersson, 1976; Khoury et al., 1985). It is an irrecoverable strain due to the physical disintegration and chemical reactions that take place in the cement paste for temperatures up to 300–400 °C, together with the thermomechanical damage of concrete produced by the thermal incompatibility between cement paste and aggregates for higher temperatures (Schneider, 1976; Mindeguia et al., 2013; Thelandersson, 1974). For these reasons, and based on empirical research, LITS is commonly regarded, and modeled, as a quasi-instantaneous strain component which develops only on first heating under load, i.e. it does not recover on cooling or develop further on reheating unless the first heating temperature is exceeded (Mindeguia et al., 2013; Thelandersson, 1974; Petkovski and Crouch, 2008; Colina and Sercombe, 2004; Illston and Sanders, 1973; Parrott, 1979). For a full description of LITS and survey of previous studies, see the recent review by Torelli et al. (2016).

A common method for modeling LITS in the case of uniaxial loading is to assume its development on first heating depends only on temperature and stress: $\varepsilon_{lits}(\sigma, T)$. LITS is generally assumed to be linear with the stress level, defined as the ratio between the compressive stress σ and the compressive strength σ_{u0} of the material, and strongly nonlinear with temperature (Anderberg and Thelandersson, 1976; Mindeguia et al., 2013; Khoury et al., 1985). Among published models, the evolution of LITS with temperature has been formulated directly, expressing the LITS as a polynomial function of the temperature (Terro, 1998; Pearce et al., 2004; Nielsen et al., 2002; Li and Purkiss, 2005), or indirectly, assuming LITS to be directly proportional to the FTS (Anderberg and Thelandersson, 1976). Whilst it is more practical, an indirect formulation of LITS seems to contrast with some experiments, where the LITS and FTS functions of temperature have been proved not to be proportional for some types of concrete (Petkovski and Crouch, 2008).

Normally, 3D LITS models are obtained from uniaxial models by assuming that if concrete is heated while compressed in one direction, it develops expansive LITS in the two directions perpendicular to the compression (Mindeguia et al., 2013; Petkovski and Crouch, 2008; Kordina et al., 1986). This leads to a constitutive formulation where the proportionality between the stress tensor and LITS increment tensor depends on an additional material coefficient, ν_{LITS} . This is defined as the negative ratio of transverse to axial LITS strain (De Borst and Peeters, 1989; Pearce et al., 2004; Gawin et al., 2004; Khennane and Baker, 1992; Thelandersson, 1987; Gernay et al., 2013). Such models rely on the superposition principle, i.e., the state of LITS caused by a multiaxial compressive stress state is assumed to be equal to the sum of the states of LITS which would have been caused by each stress component individually.

In fact, a critical analysis of the few multiaxial LITS tests available in the literature reveals that the development of LITS does not follow the superposition principle exactly. Specifically, for multiaxial stress states, LITS strains are significantly bigger than those predicted by superimposing the LITS produced by each stress component individually (Petkovski and Crouch, 2008; Kordina et al., 1986; Thienel and Rostásy, 1996; Ehm and Schneider, 1985). In other words, the triaxial development of LITS depends on the confinement of the stress state. In the light of this, this paper presents a novel 3D LITS constitutive model which captures the experimentally observed confinement-dependency of LITS and its numerical implementation. Experimental results for multiaxial LITS currently exist for temperatures up to 250 °C and these results are incorporated in the model. For temperatures higher than 250 °C, assumptions must be made about multi-axial LITS behavior. However, the method for extending uniaxial LITS curved to 3D is formulated so

future results can be added to it. Following the presentation of the LITS model, it is applied to an indicative problem – that of a nuclear PCPV vessel under heating due to fault conditions. It is shown that failing to use an accurate multiaxial-LITS model for such problems, may lead to non-conservative estimates of the stress and strain states.

2. LITS model

2.1. Confinement-based modeling approach

This section aims to present a novel approach for a 3D implementation of uniaxial temperature-LITS functions.

2.1.1. Traditional approach

Uniaxial LITS curves are commonly extended to 3D by assuming that the behavior of concrete heated under mechanical load does not depend on the confinement of the stress state (De Borst and Peeters, 1989; Pearce et al., 2004; Gawin et al., 2004; Khennane and Baker, 1992; Thelandersson, 1987; Gernay et al., 2013):

$$\dot{\varepsilon}_{ij}^{lits} = \frac{\beta(T)}{\sigma_{u0}} \left(-\nu_{lits} \sigma_{kk}^- \delta_{ij} + (1 + \nu_{lits}) \sigma_{ij}^- \right) \dot{T} \quad (2.1)$$

where $\dot{\varepsilon}_{ij}^{lits}$ is the i th j th component of the time derivative of the LITS tensor; $\beta(T)$ is the LITS derivative function, i.e. a function of temperature which describes the derivative of LITS with respect to temperature for a given stress level; σ_{u0} the concrete uniaxial compressive strength; σ_{ij}^- the i th j th component of the negative projection of the stress tensor; ν_{lits} a material parameter defined as the negative ratio of transverse to axial LITS strain, analogous to the elastic Poisson's modulus ν ; and \dot{T} , the time derivative of temperature. Considering the negative projection of the stress tensor in Eq. (2.1) ensures LITS is produced by only the compressive stress components, as required. The total number of material parameters involved in a 3D LITS model is given by the sum of the parameters included in the LITS derivative function $\beta(T)$ and the ones needed in its 3D implementation. As evident from Eq. (2.1), two material parameters are introduced when a uniaxial LITS curve is extended to 3D through the traditional approach: the concrete compressive strength σ_{u0} and the LITS Poisson's modulus ν_{lits} .

2.1.2. LITS dependency on the stress confinement

The traditional formulation described in (2-1) is based on the assumption that the LITS state produced by a multiaxial compressive stress states is the sum of the LITS states produced by uniaxial loads individually. However, this assumption contrasts with the experimentally observed concrete behavior in the case of multiaxial stress states, which show that the degree of LITS depends on the stress confinement (Petkovski and Crouch, 2008; Kordina et al., 1986; Thienel and Rostásy, 1996; Ehm and Schneider, 1985). This is exemplified by Fig. 1, which shows that the LITS obtained in Petkovski and Crouch (2008) for equal biaxial and hydrostatic compression in the loaded and unloaded directions is significantly greater than the one predicted through the superposition principle. Specifically, the underestimation of LITS obtained through the superposition principle is greater for hydrostatic than for equal biaxial compression, suggesting that LITS state grows with the stress confinement.

To date, the precise mechanisms behind the confinement dependency of LITS are not fully understood. Based on experimental evidence, such a phenomenon could be explained by postulating the confinement-dependency of two of the mechanisms underlying LITS: micro cracking effect and micro diffusion.

Micro cracking effect is commonly considered to be a source of drying creep (Bazant, 1994; Bazant and Chern, 1985; Bazant and Raftshol, 1982; Cohen et al., 1990), i.e. the excess in creep

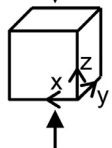
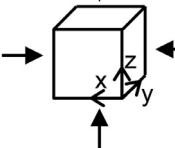
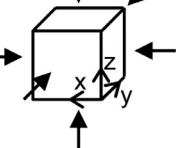
Uniaxial compression	Equal biaxial compression	Hydrostatic compression
		
LITS measured $\varepsilon_{z,lits}^{uni} = -1.56 \%$ $\varepsilon_{y,lits}^{uni} = 0.53 \%$	LITS measured $\varepsilon_{z,lits}^{bia} = -1.53 \%$ $\varepsilon_{y,lits}^{bia} = 1.76 \%$	LITS measured $\varepsilon_{z,lits}^{hyd} = -1.06 \%$
LITS predicted (superp. principle) $\varepsilon_{z,lits}^{uni} = -1.56 \%$ $\varepsilon_{y,lits}^{uni} = 0.53 \%$	LITS predicted (superp. principle) $\varepsilon_{z,lits}^{bia} = -1.03 \%$ $\varepsilon_{y,lits}^{bia} = 1.06 \%$	LITS predicted (superp. principle) $\varepsilon_{z,lits}^{hyd} = -0.50 \%$

Fig. 1. Comparison between the LITS measured for uniaxial, equal biaxial and hydrostatic compression for $\sigma/\sigma_{u0} = 0.47$ and $T = 250^\circ$ (Petkovski and Crouch, 2008) and the values predicted for biaxial and hydrostatic compression through the superposition principle, starting from the measured uniaxial LITS.

that develops in drying concrete with respect to sealed concrete (Pickett, 1942). Being drying creep a component of LITS, the micro cracking mechanism also affects the development of the latter. When unloaded concrete dries, micro cracks develop due to the non-homogeneity of moisture content, evaporation and evacuation, which determine an overall expansion of the material. However, if a uniaxial compressive load is applied, micro cracks are prevented from developing on planes orthogonal to the direction of compression, leading to the measurement of a compaction strain component in the loaded direction (Bazant, 1994; Bazant and Chern, 1985). The apparent excess in LITS measured in the loaded directions in the case of biaxial compression may be partially explained by the fact that micro cracks are prevented from developing on planes orthogonal to the two loaded direction. This leads to bigger compressive strains than the ones obtained through the superposition of two LITS states produced by uniaxial load, where in contrast cracks occur in all the planes parallel to the compressive load. Besides, the apparent excess in LITS strain measured in the unloaded direction in the case of biaxial compression may be due to a significant development of micro cracks on the planes orthogonal to the unloaded direction, promoted by the simultaneous presence of a compressive load in the other two directions. Similarly, the excess in LITS for hydrostatic compression may be justified by a nearly complete absence of micro cracks due to the high confinement of the material.

Another mechanism underlying LITS is micro diffusion, that is the exchange of water between micro pores (gel pores) and macro pores (capillary pores) (Bazant, 1994). In the case of loaded concrete drying at constant temperature, this phenomenon is induced by a loss of macro pore water. Such mechanism is also considered to be a source of transient thermal creep, defined as the LITS developing in absence of drying. In this case, micro diffusion may be due to the temperature-induced increase in micro pore pressure in the case of concrete heated under sealed conditions (Petkovski and Crouch, 2008). Accordingly, a possible explanation of the apparent excess in experimentally observed LITS for high hydrostatic compressive stress components, with respect to the LITS predicted by the superposition principle, might be the confinement-induced

Table 1

Triaxiality index C_m and confinement coefficient η obtained for three different exemplifying values of triaxiality scaling factor ($\gamma = 0$, $\gamma = 0.5$, $\gamma = 1$ and $\gamma = 1.5$) in the case of uniaxial, equal biaxial and hydrostatic compressive stress states.

Stress state	C_m	$\eta(\gamma = 0)$	$\eta(\gamma = 0.5)$	$\eta(\gamma = 1)$	$\eta(\gamma = 1.5)$
Uniaxial	1	1	1	1	1
Equal biaxial	1.41	1	1.21	1.41	1.62
Hydrostatic	1.73	1	1.37	1.73	2.10

increase in micro pore pressure. This can be due to a higher reduction in volume of the gel pores in the case of multiaxial compressive stress states then in the case of uniaxial compression.

However, the confinement dependency of micro diffusion and micro cracking remain to be demonstrated.

2.1.3. Confinement-based approach

The discussion of the dependency of LITS on the stress confinement reported in Section 2.1.2 suggests that LITS can be modeled as a confinement dependent strain. In the light of this, a new approach for extending uniaxial LITS curves to 3D is presented. Specifically, the strain evaluated through Eq. (2.1) is multiplied by a confinement coefficient η aimed at amplifying the LITS evaluated through the superposition principle so as to fit the experimentally measured strains:

$$\dot{\varepsilon}_{ij}^{lits} = \eta \frac{\beta(T)}{\sigma_{u0}} (-\nu_{lits} \sigma_{kk}^- \delta_{ij} + (1 + \nu_{lits}) \sigma_{ij}^-) \dot{T} \quad (2.2)$$

where η is defined as a function of a triaxiality index C_m :

$$\eta = 1 + (C_m - 1)\gamma \quad (2.3)$$

$$C_m = \frac{|\sigma_1^- + \sigma_2^- + \sigma_3^-|}{\sqrt{(\sigma_1^-)^2 + (\sigma_2^-)^2 + (\sigma_3^-)^2}} \quad (2.4)$$

where σ_1^- , σ_2^- and σ_3^- are the negative projections of the principal stresses and γ is the triaxiality scaling factor, which is the only additional material parameter introduced with respect to the traditional method described by Eq. (2.1).

C_m is an index allowing the triaxiality of all the compressive parts of stress states to be captured. Table 1 shows that C_m grows with increasing triaxiality of the stress state: it equals 1 for uniaxial compression and it assumes values greater than 1 for biaxial and triaxial compression. As shown from Eq. (2.3), the triaxiality scaling factor γ is a material parameter describing the sensitivity of the development of LITS to the triaxiality of the stress state, allowing translation of C_m into the confinement coefficient η . In other words γ should be calibrated so that η fits the ratio between the experimentally measured LITS and the prediction obtained via the traditional approach. Table 1 shows that the values assumed by confinement coefficient η grow with the triaxiality scaling index γ . If $\gamma = 0$, then $\eta = 1$ and is independent of the stress state, i.e. the LITS dependency on the stress confinement is not taken into account and the (2-2) reduces to the (2-1). As shown in section 3.3, based on the experiments on multiaxially compressed concrete heated up to 250°C reported in Petkovski and Crouch (2008), the authors suggest a triaxiality scaling factor of $\gamma = 1.5$. However, if new experiments involving different concrete mixtures were performed, further studies on the calibration of the parameter could be adopted. If, for example, for specific concrete mixtures the LITS dependency on confinement was found to be different for different temperature ranges, γ could be defined as a function of the temperature, therefore allowing the approach described in the (2-2), (2-3) and (2-4) to capture such a dependence. Thus the approach adopted here can be used based on current experimental data but is also flexible enough to account for future findings.

2.2. Bilinear LITS derivative function

In this section, the main advantages and disadvantages of the uniaxial LITS models available in the literature are first discussed. Then, an original bilinear uniaxial model is proposed, which allows to capture the triaxial development of LITS better than the others when extended to 3D for temperatures up to 250 °C.

For uniaxial loading conditions, LITS is usually modeled as a temperature and stress dependent strain as follows:

$$\dot{\epsilon}^{lits} = \beta(T) \frac{\sigma}{\sigma_{u0}} \dot{T} \tag{2.5}$$

Where $\dot{\epsilon}^{lits}$ is time derivative of LITS; $\beta(T)$ the LITS derivative function, σ the compressive stress for uniaxial conditions, σ_{u0} the concrete compressive strength of the material and \dot{T} , the time derivative of temperature. The general approach described by Eq. (2.2) can be used to extend to 3D any uniaxial LITS curve expressed in the form (2.5). This can be done by introducing the LITS derivative function $\beta(T)$, defined for uniaxial conditions in Eqs. (2.5) and (2.2).

A simple uniaxial model expressed in the form (2.5) available in the literature is the one proposed by Anderberg and Thelandersson (1978), which assumes the LITS and FTS curves to be directly proportional:

$$\dot{\epsilon}^{lits} = k_{tr} \alpha(T) \frac{\sigma}{\sigma_{u0}} \dot{T} \tag{2.6}$$

Where k_{tr} is a material parameter defining the proportionality between the two curves. This model presents the advantage of involving a single material parameter. However, the assumption of a linear proportionality between LITS and FTS seems to contrast with experimental results obtained for different types of concrete (Colina and Sercombe, 2004; Hassen and Colina, 2006; Colina et al., 2004). These experiments show that modeling LITS independently to the FTS represents a more generic approach.

For this reason, many uniaxial models have been proposed in the past, where LITS is formulated as a polynomial function of temperature by curve-fitting the uniaxial tests (Anderberg and Thelandersson, 1976; Terro, 1998; Nielsen et al., 2002; Li and Purkiss, 2005). Nevertheless, although a good fit is achieved for uniaxial test data, these models generally fail to capture the evolution of LITS for multiaxial stress states if extended to 3D. This is because, as shown from Fig. 8b–d, the LITS developing along loaded and unloaded directions for different loading conditions cannot be always considered directly proportional to the uniaxial curve, i.e. they have different shapes (Petkovski and Crouch, 2008).

Therefore the benefits of accurately fitting the uniaxial curve, if multiaxial stress states have to be studied, are unclear. In this case, a uniaxial model which aims to represent the general trend of the LITS curves in the loaded and unloaded directions, for uniaxial, biaxial and hydrostatic compression, appears to be more suitable than a model which only fits the uniaxial LITS curve accurately.

A comparison of the LITS curves obtained in Petkovski and Crouch (2008) for loaded and unloaded directions, for various loading conditions and temperatures up to 250 °C, allowed the following features to be identified:

- LITS does not develop significantly for temperatures lower than 100 °C. This suggests the definition of a model where the temperature needs to exceed a threshold value in order for LITS to develop.
- Above 100 °C, the evolution of LITS varies depending on the considered direction and stress conditions. In particular, the curves present slightly different trends. Thus, the most appropriate approximation to capture the general LITS evolution in this region appears to be a linear function.

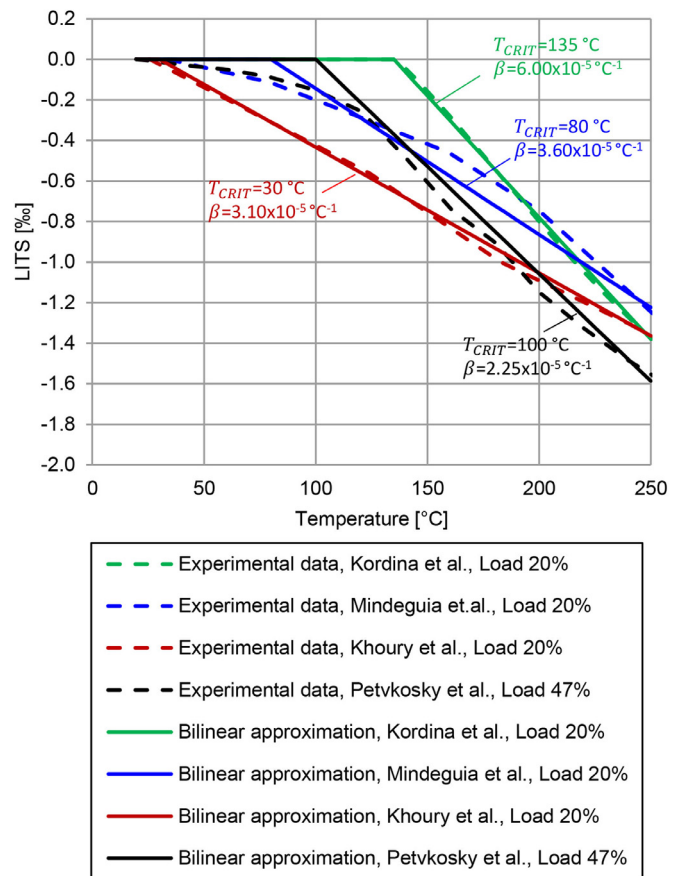


Fig. 2. Bilinear approximations of experimental LITS curves obtained (Kordina et al., 1986; Mindeguia et al., 2013; Khoury et al., 1985; Petkovski and Crouch, 2008) for various load levels σ/σ_{u0} .

In addition, an analysis of the existing experiments under uniaxial compressive states confirms that, for temperatures below 250 °C, LITS may be modeled with a reasonable accuracy as a bilinear function of the temperature – see Fig. 2.

With this in mind, a bilinear uniaxial model, conceived to be extended to 3D and governed by only two material parameters, is presented here as follows:

$$\begin{cases} \dot{\epsilon}^{lits} = 0 & \text{for } T \leq T_{CRIT} \\ \dot{\epsilon}^{lits} = B \frac{\sigma}{\sigma_{u0}} \dot{T} & \text{for } T > T_{CRIT} \end{cases} \tag{2.7}$$

where T_{CRIT} and B are material parameters representing the critical temperature that the material needs to reach in order for LITS to develop and a constant LITS derivative coefficient respectively. In other words, T_{CRIT} is the temperature at which LITS is found to develop significantly, through experiments; B defines the increment in LITS corresponding to a unit increment in temperature, normalized with respect to the load level σ/σ_{u0} , for temperatures higher than T_{CRIT} .

2.3. Model implementation

The model has been implemented within the general framework of the finite element code Code_Aster (De Soza, 2013), through the code generator MFront (Helfer et al., 2015).

2.3.1. Implementation of LITS

The LITS model has been obtained by using the approach described in Section 2.1 to extend the bilinear model defined in

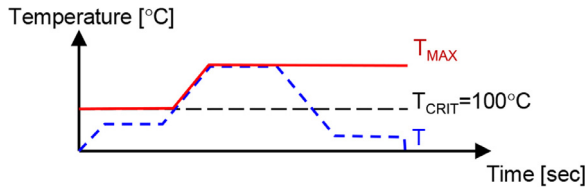


Fig. 3. Schematic evolution of the internal variable T_{MAX} , for a given temperature history and a critical temperature T_{CRIT} .

Sections 2.2 to 3D and by imposing LITS to be irrecoverable in terms of temperature.

The combination of Eqs. (2.2) and (2.7) and gives:

$$\begin{cases} \dot{\varepsilon}_{ij}^{lits} = 0 & \text{for } T \leq T_{CRIT} \\ \dot{\varepsilon}_{ij}^{lits} = \eta \frac{B}{\sigma_{u0}} (-\nu_{lits} \sigma_{kk}^- \delta_{ij} + (1 + \nu_{lits}) \sigma_{ij}^-) \dot{T} & \text{for } T > T_{CRIT} \end{cases} \quad (2.8)$$

Furthermore, LITS has been implemented in a way that it develops just on first heating, i.e. it is not only temperature dependent, but also temperature history dependent. This has been obtained by the introduction of a variable T_{MAX} , which is defined as the maximum of T_{CRIT} and the maximum temperature ever reached by the material. As an example, Fig. 3 shows the evolution of T_{MAX} for a given critical temperature T_{CRIT} and temperature history: it assumes the value T_{CRIT} at the beginning of the calculation and stores the maximum reached temperature if the critical temperature T_{CRIT} is exceeded. LITS irrecoverability over cooling or reheating to temperatures lower than T_{MAX} was implemented by imposing that $T_{MAX} = T_{CRIT}$ is a necessary condition for LITS to develop, leading to:

$$\begin{cases} \dot{\varepsilon}_{ij}^{lits} = 0 & \text{for } T < T_{MAX} \\ \dot{\varepsilon}_{ij}^{lits} = \eta \frac{B}{\sigma_{u0}} (-\nu_{lits} \sigma_{kk}^- \delta_{ij} + (1 + \nu_{lits}) \sigma_{ij}^-) \dot{T} & \text{for } T = T_{MAX} \end{cases} \quad (2.9)$$

Therefore, for a specific time step, the increment $\Delta \bar{\varepsilon}_{lits}$ in LITS tensor was defined as:

$$\begin{cases} \Delta \bar{\varepsilon}_{lits} = 0 & \text{for } T \leq T_{CRIT} \\ \Delta \bar{\varepsilon}_{lits} = \eta \left[\frac{B}{\sigma_{u0}} \right] ((1 + \nu_{lits}) \bar{\sigma}_m^- - \nu_{lits} tr(\bar{\sigma}_m^-) \bar{I}) \Delta T & \text{for } T \geq T_{CRIT} \end{cases} \quad (2.10)$$

where $\bar{\sigma}_m^-$ is the mean value of the negative projection of the stress tensor at the beginning and at the end of the time step.

In a similar manner, the triaxiality index C_m defined in Eq. (2.4) was implemented with respect to the principal stresses of $\bar{\sigma}_m^-$:

$$C_m = \frac{|\sigma_{1,m}^- + \sigma_{2,m}^- + \sigma_{3,m}^-|}{\sqrt{(\sigma_{1,m}^-)^2 + (\sigma_{2,m}^-)^2 + (\sigma_{3,m}^-)^2}} \quad (2.11)$$

where $\sigma_{1,m}^-$, $\sigma_{2,m}^-$ and $\sigma_{3,m}^-$ are the principal stresses of $\bar{\sigma}_m^-$.

2.3.2. General strain decomposition

The LITS component defined in Eq. (2.10) has been embedded in a simple thermoelastic material behavior law, leading to the following expression of strain decomposition:

$$\Delta \bar{\varepsilon}_{tot} = \Delta \bar{\varepsilon}_{el} + \Delta \bar{\varepsilon}_{th} + \Delta \bar{\varepsilon}_{lits} \quad (2.12)$$

Where $\Delta \bar{\varepsilon}_{tot}$, $\Delta \bar{\varepsilon}_{el}$, $\Delta \bar{\varepsilon}_{th}$ and $\Delta \bar{\varepsilon}_{lits}$ are the increment in total strain, elastic strain, FTS and LITS respectively:

$$\Delta \bar{\varepsilon}_{el} = \frac{1 + \nu}{E} \Delta \bar{\sigma} - \frac{\nu}{E} tr(\Delta \bar{\sigma}) \bar{I} \quad (2.13)$$

$$\Delta \bar{\varepsilon}_{th} = \alpha \Delta T \bar{I} \quad (2.14)$$

where $\Delta \bar{\sigma}$ is the increment in stress tensor, \bar{I} is the identity matrix and, E the Young's modulus, ν the Poisson's ration and α , the coefficient of thermal expansion, which can be defined as a function of the temperature.

According to the LITS definition given in Section 1, the presented LITS model contains all the strain components developing in loaded concrete during a thermal transient. Thus, it includes:

- the increment in elastic strain due to the degradation of the elastic properties on heating,
- drying and basic creep,
- TTC.

It should be noted that in the presented model the temperature-induced increment in elastic strain is implicitly included in the LITS component. Accordingly, the elasticity material parameters E and ν have to be kept constant with the temperature, so as to avoid taking into account the elastic contribution twice.

The LITS model presented in Eq. (2)–(10) could also be included in a more comprehensive constitutive law, such as a damage-plasticity model, allowing also the nonlinear mechanical material behavior connected to concrete cracking and crushing to be captured. Moreover, if the long-term behavior of the material has to be represented, an isothermal creep component could be added, aimed at modeling development of delayed strains before and after the thermal transient. In this case, the general strain decomposition would be as follows:

$$\Delta \bar{\varepsilon}_{tot} = \Delta \bar{\varepsilon}_{el} + \Delta \bar{\varepsilon}_d + \Delta \bar{\varepsilon}_{pl} + \Delta \bar{\varepsilon}_{cr} + \Delta \bar{\varepsilon}_{th} + \Delta \bar{\varepsilon}_{lits} \quad (2.15)$$

Where $\Delta \bar{\varepsilon}_d$ represents the strain component due to the mechanical damage of the material, $\Delta \bar{\varepsilon}_{pl}$ the plastic strain and $\Delta \bar{\varepsilon}_{cr}$ the time dependent isothermal creep strain.

In this work, embedding the newly formulated LITS component in a thermoelastic material law, as described by, (2.13) and (2.14), was deemed to be appropriate. This allowed to verify the LITS model itself, validate it against experiment performed at relatively low stress levels – therefore not involving material nonlinearities connected to cracking and crushing – and capture the influence of LITS on the behavior of PCPVs subjected to accidental conditions.

LITS is here modeled as a stress and temperature history dependent phenomenon. Further experimental and numerical work needs to be done to assess and model the effect of moisture movement on LITS.

2.3.3. Numerical methods

The static nonlinear problem is solved by discretizing the time and evaluating the equilibrium of the structure at each considered instant i (Zienkiewicz, 1977; EDF 2013). At each time step, the equilibrium is searched by looking for the displacements satisfying the mechanical equilibrium at a structural level. This is done here through a *Newton-Raphson* iterative method with tangent matrix prediction, allowing to obtain an estimation of the displacement and to verify if the corresponding internal forces satisfy the equilibrium, at each iteration. The iterative method stops when the internal forces satisfy the equilibrium (Zienkiewicz, 1977; EDF 2013).

At the n -th iteration of the iterative method, the vector of the internal forces at the end of the time-step \bar{F}_i^{int} is evaluated as a function of the estimated displacements $\bar{V}_{i,n}$ through the mechanical behavior. First, the estimated strain increment $\Delta \bar{\varepsilon}_{tot}$ at each gauss point is evaluated as a function of the estimated displacements $\bar{V}_{i,n}$. Then, constitutive relationship provides, at each gauss point, an estimation of the stress tensor $\bar{\sigma}$ and the values of some internal variables at the end of the time step, as a function of the estimated strain increment $\Delta \bar{\varepsilon}_{tot}$. The vector of the internal forces

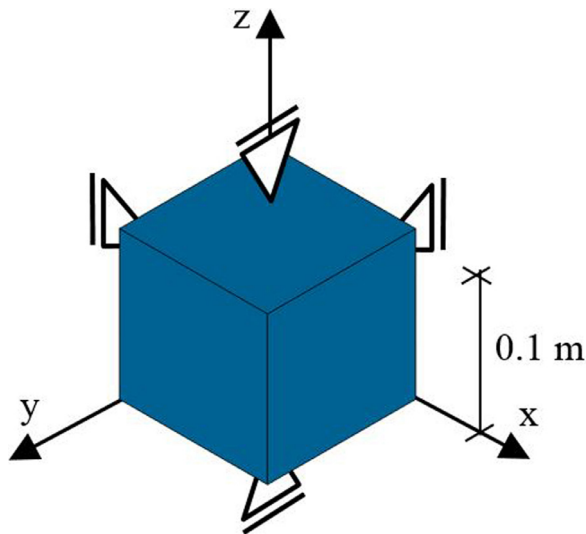


Fig. 4. Mesh and kinematic conditions adopted for modeling a uniaxially restrained concrete specimen.

at the end of the time-step \bar{F}_i^{int} is finally evaluated as a function of the stress tensors $\bar{\sigma}$ (EDF 2013).

The local integration of the material behavior law is performed using an implicit scheme based on a standard *Newton–Raphson* algorithm and a jacobian matrix computed by a second order finite difference (Helfer et al., 2015).

3. Verification and validation studies

In order to verify and validate the constitutive model presented in Section 2, a series of numerical test cases investigating the effects of heating-cooling cycles on concrete specimens subjected to various mechanical boundary conditions were designed.

First, the stress state of a hypothetical uniaxially restrained specimen subjected to multiple heating-cooling cycles was studied in order to verify the model, i.e. to confirm that the model presented in Section 2 was correctly implemented in the FE code.

Then, the model was calibrated and validated against multiaxial transient tests performed within the experimental campaign presented in Petkovski and Crouch (2008). Specifically, the bilinear LITS curve parameters B , T_{crit} and v_{lits} were calibrated by fitting the uniaxial LITS test in the loaded and unloaded directions, while the triaxiality scaling factor γ was defined so as to capture the apparent excess in LITS in the case of multiaxial compression discussed in 2.1.2. The calibrated model was next validated by modeling transient tests performed under biaxial and triaxial compression.

3.1. Uniaxially restrained specimen

3.1.1. FE model

First, the case of a uniaxially restrained cubic specimen was considered. This was modeled using a single element with an arbitrary edge length of 0.1 m. The element was subjected to uniaxially restrained thermal strain was considered to verify the constitutive law in the case of strain-controlled conditions, i.e. varying stresses. As shown from Fig. 4, a mesh composed of one hexahedral element with 8 nodes was defined and four of the six faces were prevented from moving in their normal direction so as to allow strains to develop along the directions x and y , but not along z . As shown from Fig. 5, the material was first subjected to two consecutive heating-cooling cycles, up to 140 °C and 180 °C respectively, and then heated up to 220 °C. The transient temperature was modeled by assigning the same thermal history to all the 8 nodes of

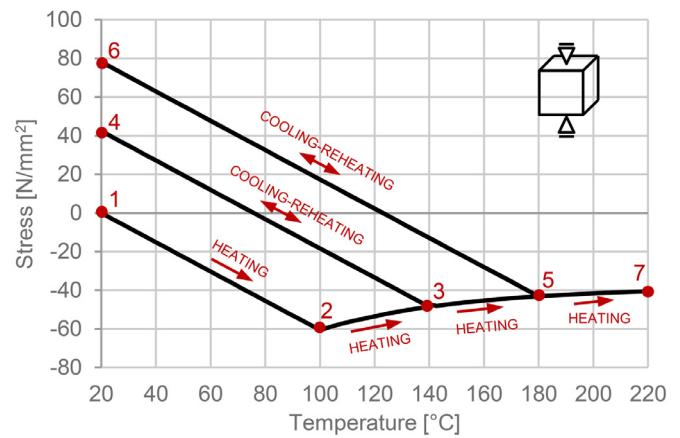


Fig. 5. Uniaxially constrained specimen subjected to multiple heating cooling cycles: applied thermal load and evolution of the stress in the constrained direction, obtained with a bilinear LITS function.

Table 2

Uniaxially restrained specimen: material parameters.

Parameter	Value
E	47,000 MPa
ν	0.25
A	$1.62 \times 10^{-5} \text{ } ^\circ\text{C}^{-1}$
B	$2.38 \times 10^{-5} \text{ } ^\circ\text{C}^{-1}$
γ	1
σ_{u0}	57 MPa
v_{lits}	0.37
T_{crit}	100 °C

the model. The constitutive law presented in Section 2 was defined with the material parameters in Table 2. For ease of interpretation of the results, a constant coefficient of thermal strain, α , was used.

3.1.2. Results and discussion

The results, in terms of thermal evolution of the stress along z -axis with the temperature, are shown in Fig. 5. On heating, stresses develop along z -axis, due to the constrained thermal strain. Since the coefficient of thermal strain is constant with temperature, the stress grows linearly with temperature until 100 °C (point 2 in Fig. 5), the value of T_{CRIT} . For higher temperatures, LITS starts developing producing a stress relaxation (point 2 to point 3) which is not recovered on cooling (point 3 to point 4). In fact, the stress decreases linearly with temperature, since only the component due to restrained thermal strain is recovered. Similarly, the stress increases linearly, following the heating cooling branch from point 2 to point 3, when the material is subsequently re-heated up to the maximum temperature reached in the first cycle, stored by the variable T_{MAX} , of 140 °C. When this temperature is exceeded, the material start relaxing again, due to the re-activation of LITS (point 3 to point 5). A similar behavior is obtained on subsequent cooling (point 5 to point 6) and heating to 220 °C (point 6 to point 7).

The model's ability to capture LITS taking place in restrained elements subjected to transient high temperatures is thus shown. In addition, the LITS irrecoverability on cooling is demonstrated.

3.2. Multiaxially loaded specimens

The model was next used to numerically simulate the experimental results for LITS in multiaxial compressive stress states and temperatures up to 250 °C reported by Petrovski et al (Petkovski and Crouch, 2008). These numerical studies were performed to verify the proposed model in the case of stress-controlled tests, to

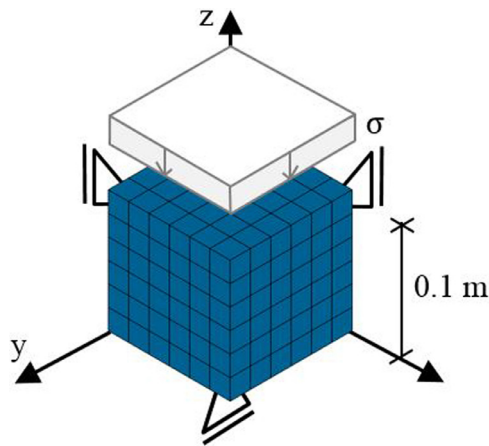


Fig. 6. Mesh and kinematic conditions adopted for modeling the concrete specimens tested in Petkovski and Crouch (2008): case of uniaxial compression.

validate it against experimental evidence, and to calibrate its material parameters.

3.2.1. Reference experiments

Petrovski et al's experimental tests (Petkovski and Crouch, 2008) were performed on the *mac^{2T}* apparatus at the University of Sheffield, a facility for testing 100 mm cubic concrete specimens under multiaxial compression and high temperatures. Compressive stresses up to 400 MPa can be applied in the three directions independently, and temperature up to 300 °C can be imposed. The stress states can be applied to specimens' faces through six steel platens, which are also able to transfer heat to the concrete by conduction.

In the tests replicated here, uniaxial, equal biaxial and hydrostatic compression were applied. Specifically a compressive stress of 27 MPa was applied along the loaded directions, while a relatively small confining pressure of 1 MPa was applied along the unloaded directions. Then, a heating-cooling cycle up to 250 °C was imposed while the mechanical load was being kept constant.

3.2.2. FE models

The mesh and kinematic conditions adopted for modeling the concrete specimens are shown in Fig. 6, where the pressure applied for modeling the case of uniaxial compression is also represented. The specimens were modeled by 216 hexahedric elements with 8 nodes. Three faces were prevented from moving along their normal directions to prevent rigid body motion while allowing strains to develop along in all directions. To reproduce the real evolution of the temperature field through the specimens, the temperature history reported in Fig. 7 was applied to the nodes on the external surfaces, while the temperature of the inner nodes was calculated by a linear thermal analysis. A thermal conductivity $\lambda = 0.70 \text{ W m}^{-1} \text{ K}^{-1}$ and a specific heat capacity $\rho_{cp} = 6.2 \times 10^6 \text{ J m}^{-3} \text{ K}^{-1}$ were used, after calibration through a parametric study aimed at fitting the experimental curve describing the evolution of the temperature in the centroid of the specimen when the temperature of the platens rises linearly at a rate of 2 °C/min, as reported in Petkovski and Crouch (2008). In order to verify the behavior of the implemented model on reheating in the case of stress controlled conditions, an additional heating phase to 250 °C (not present in the experiments) was numerically modeled in the present study, as shown in Fig. 7 for the case of uniaxial compression. The thermal strain coefficient function $\alpha(T)$ was defined as the derivative with respect to temperature of the FTS curve experimentally obtained in Petkovski and Crouch (2008).

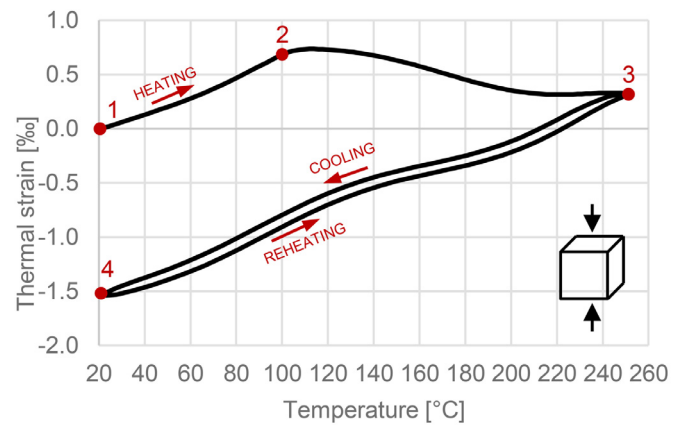


Fig. 7. Uniaxially loaded specimen subjected to heating-cooling-heating cycle: evolution of the thermal strain (FTS+LITS) in the loaded direction obtained with the bilinear LITS function.

Fig. 8a shows the match between experimental and numerical FTS curve.

For the LITS model, three different values of triaxiality scaling factor γ were considered:

- $\gamma = 0$, representing the limit case where the confinement dependent approach described by equation (2-2) reduces to the traditional approach described by Eq. (2.1),
- $\gamma = 1$, for which confinement coefficient η equals the triaxiality index C_m ,
- $\gamma = 1.5$, which was found to be the value which gives the most suitable values of η for fitting the equal biaxial and hydrostatic tests, though a parametric study.

The mechanical material parameters T_{CRIT} , B and ν_{LITS} were calibrated to fit the uniaxial LITS curves. Since LITS was found to develop significantly only above 100 °C, a critical temperature $T_{CRIT} = 100 \text{ °C}$ was defined. Then, for each considered value of γ , the parameter B was calibrated so as to fit the uniaxial LITS curve in the loaded direction. Subsequently ν_{LITS} was calibrated to fit the transversal LITS. The calibrated parameters were next used to predict the response in the case of equal biaxial and hydrostatic compression. It should be noted that in the case of pure uniaxial compression, LITS in the loaded and unloaded direction does not depend on the triaxiality scaling factor γ , since according to equation (2-3) the confinement coefficient assumes the value $\gamma = 1$ regardless. Therefore, a unique value of the parameter B would allow the uniaxial LITS in the loaded direction to be fitted, independent of γ . However, since the considered uniaxial and equal biaxial tests were performed with a small confining pressure along the unloaded directions, slightly different values of B were needed to fit exactly the uniaxial curves for different values of γ (see Table 3).

For comparison purposes, the tests were also modeled by substituting the presented bilinear LITS model with the Anderberg and Thelandersson LITS models described by equation (2-6), implemented in 3D through the traditional approach described by Eq. (2.1). Similarly, the material parameter k_{tr} and ν_{LITS} were calibrated to fit the uniaxial LITS curves and then used to assess the LITS for multiaxial compressive states. Table 3 summarizes sets of material parameters adopted for all the considered models.

3.2.3. Results and discussion

The obtained results allowed the behavior law presented in Section 2 to be validated in the case of stress-controlled conditions. Fig. 7 shows the thermal strain (representing the sum of FTS and LITS) as a function of the temperature, obtained with the bilinear LITS model and $\gamma = 1$ in the case of uniaxial compression. At the

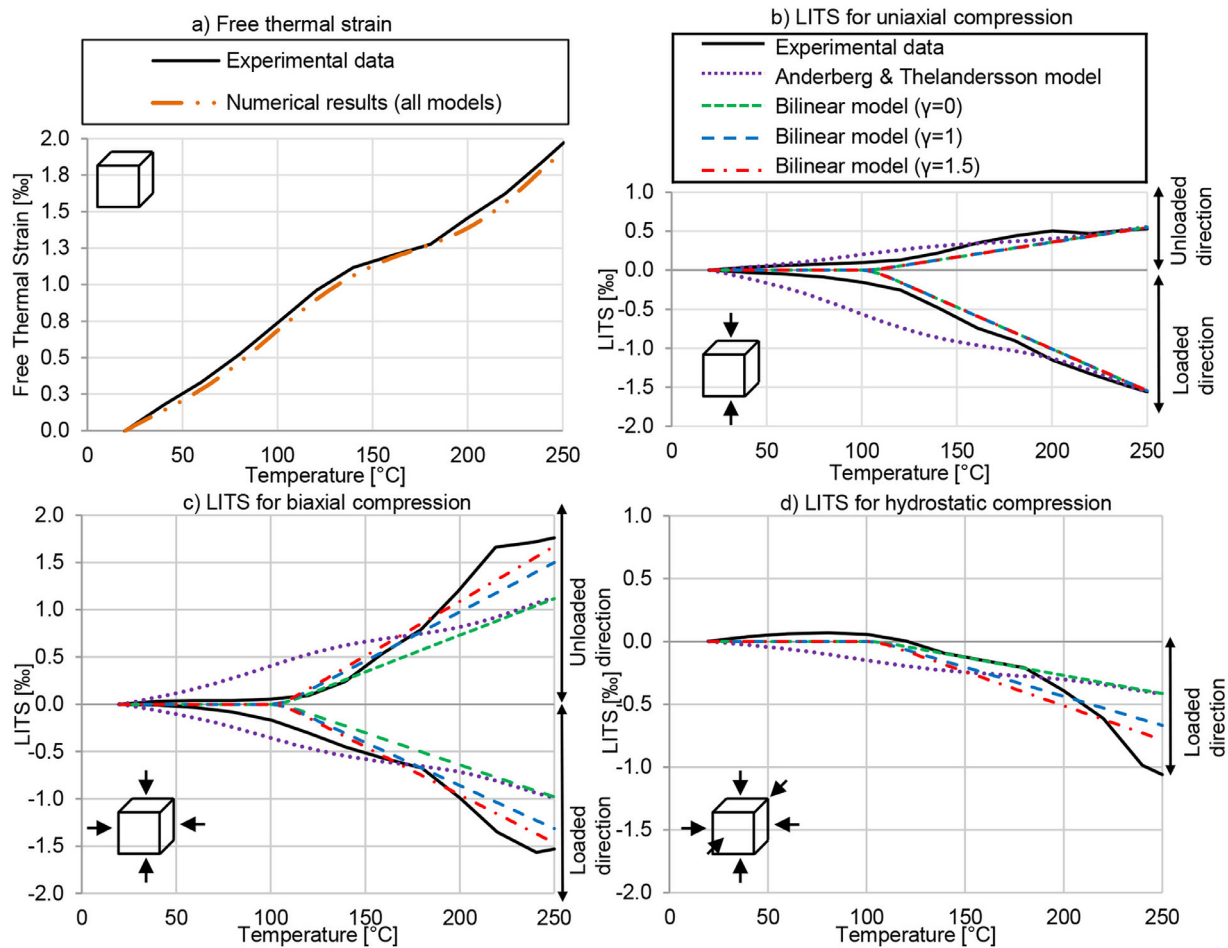


Fig. 8. Developments of FTS and LITS with temperature along the loaded and unloaded directions, for specimens subjected to biaxial and hydrostatic compression.

Table 3

Material parameters adopted for the different models used to simulate the multiaxial tests reported in Petkovski and Crouch (2008).

Parameter	Anderberg & Thelandersson	Bilinear ($\gamma=0$)	Bilinear ($\gamma=1$)	Bilinear ($\gamma=1.5$)
E	47,000 MPa	47,000 MPa	47,000 MPa	47,000 MPa
ν	0.25	0.25	0.25	0.25
k_{tr}	1.78	–	–	–
B	–	$2.33 \times 10^{-5} \text{ }^\circ\text{C}^{-1}$	$2.17 \times 10^{-5} \text{ }^\circ\text{C}^{-1}$	$2.10 \times 10^{-5} \text{ }^\circ\text{C}^{-1}$
γ	–	0	1.0	1.5
σ_{u0}	57 MPa	57 MPa	57 MPa	57 MPa
ν_{lits}	0.37	0.37	0.37	0.37
T_{crit}	–	100 °C	100 °C	100 °C

beginning of the heating phase (point 1 to point 2 in Fig. 7), concrete expands due to the development of FTS. When the critical temperature $T_{CRIT} = 100 \text{ }^\circ\text{C}$ is exceeded, LITS develops in addition to FTS (point 2 to 3). This first reduces the rate of expansion in the loaded direction and then causes the material to contract as the temperature rises. On cooling (point 3 to point 4), only the FTS component is recovered, leading to a significant overall contraction after a heating-cooling cycle. When subsequently re-heated, the material undergoes an addition FTS expansion (point 4 to 3), approximately following the cooling branch. The misalignment between cooling and heating branches observed in Fig. 7 is due to the slight delay in heating-cooling of the core of the specimen with respect to the external surfaces.

Fig. 8 summarizes the FTS and LITS curves obtained experimentally (Petkovski and Crouch, 2008) and numerically, through the Anderberg and Thelandersson LITS model (Anderberg and The-

landersson, 1976) and the confinement-dependent bilinear model proposed here. The Anderberg and Thelandersson model implemented with the traditional approach does not allow the general trend of the LITS curves to be captured. This is because the FTS develops almost linearly with the temperature whilst LITS develops significantly only for temperatures higher than $100 \text{ }^\circ\text{C}$. Therefore, this is in contrast with the model assumption of direct proportionality between the two curves. On the contrary, the introduction of the bilinear model allows to capture the general trend of the LITS curves. However, if the bilinear model is implemented through the traditional approach ($\gamma=0$), the confinement effect is still not captured and LITS for biaxial and hydrostatic compression is still underestimated. For these loading conditions, the numerical results improve significantly if the presented confinement dependent approach is adopted ($\gamma=1$ and $\gamma=1.5$). Specifically, the re-

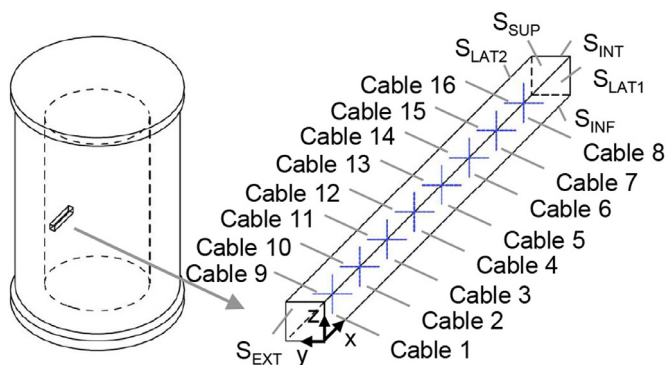


Fig. 9. Schematic illustration of a typical PCPV and model of the studied representative portion.

Table 4

Adopted material parameters for steel: Young modulus E , Poisson ratio ν and coefficient of thermal expansion α .

Parameter	Adopted value
E	47,000 MPa
ν	0.25
α	$1.62 \times 10^{-5} \text{ } ^\circ\text{C}^{-1}$

sults illustrates that the best approximations are obtained with a triaxial scaling factor $\gamma = 1.5$.

4. Test case: PCPV subjected to heating-cooling cycle

The validated and verified constitutive law was next employed to assess the loss in prestress in the tendons located at mid height of the wall of a typical nuclear PCPV, in the case of an accidental heating-cooling cycle.

4.1. FE model

As shown in Fig. 9, a cylindrical vessel having a 4.5 m thick wall was considered. A representative parallelepiped-shaped portion of the lateral wall was modeled to assess the behavior of the examined region. The considered representative portion of the vessel is 0.5 m high, 0.5 m wide and extends through the entire thickness of the wall, as shown in Fig. 9. The effect of the large radius of curvature was neglected. In addition, the anular deformative behavior of the wall at mid-height was assumed to be unaffected by the horizontal confinement effect of the top cap and foundation slab. Hence, the vessel was idealized as an infinite cylinder with respect to its behavior in the horizontal directions (Granger, 1996). Based on these assumptions, the representative portion of the wall was free to expand in the circumferential direction under the effect of transient temperatures. Expansion in the radial direction was also allowed. Accordingly, with reference to Fig. 9, only the faces S_{INT} , S_{LAT} and S_{INF} were fixed along their normal directions. As shown in Fig. 9, a prestressing system composed of 8 tangential and 8 vertical tendons was considered. The tendons were modeled explicitly by means of beam elements perfectly bonded to the concrete. An initial tension of 920 kN was applied to each tendon.

The steel tendons were modeled as a thermoelastic material. The steel material parameters are defined in Table 4. For the concrete, the confinement dependent bilinear LITS material model presented in Section 2 was employed. The material parameters calibrated against experiments, as described in Section 3.2, were adopted (see the set of parameters reported in Table 3 for $\gamma = 1.5$). For comparison, the same calculations were performed by neglect-

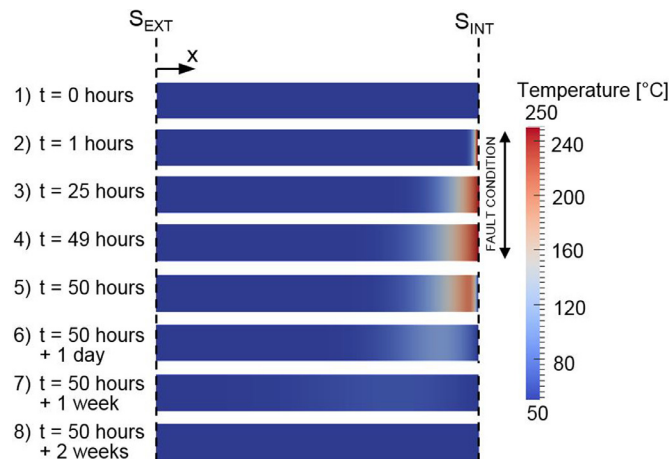


Fig. 10. Temperature profile through the thickness of the wall: before the fault ($t = 0$ h), at the end of the heating phase ($t = 1$ h), at the middle of the fault conditions ($t = 25$ h) at the beginning of the cooling phase ($t = 49$ h), at the end of the cooling phase ($t = 50$ h) and at 1 day, 1 week and 2 weeks after the end of the cooling phase.

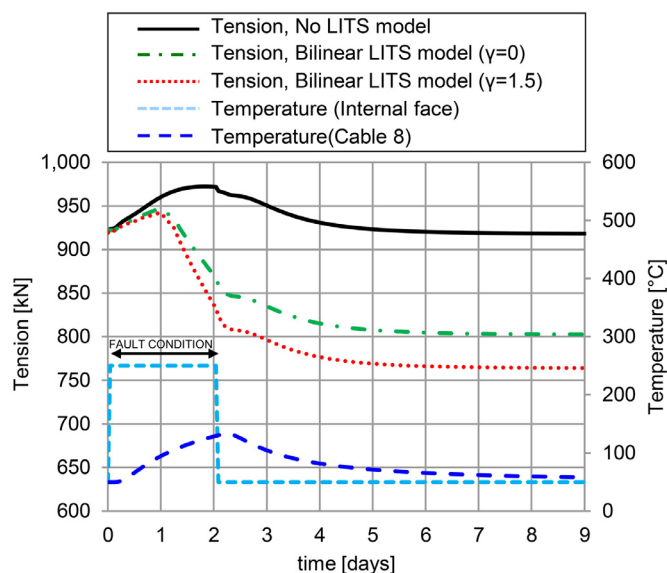


Fig. 11. Temperature histories at the internal surface and in Cable 08, and tension histories of Cable 08 without LITS, with the bilinear model with $\gamma = 1$, and with the bilinear model with $\gamma = 1.5$.

ing the confinement dependency of LITS (i.e. by adopting the set of parameters reported in Table 3 for $\gamma = 0$) and by completely deactivating the LITS component of the material behavior law.

For normal operating conditions, the temperature of concrete at the internal face of the vessel of AGRs is kept at about 50 °C by means of water cooling pipes system. In the case of a fault in the cooling system, the temperature of concrete could potentially rise to 500–600 °C, the temperature of the gas coolant for service conditions. In this study, a temporary partial fault of the cooling system was considered, making the inner surface of the vessel reach a temperature of 250 °C for 48 h. The evolution of the temperature field throughout the thickness of the wall, described in Fig. 10, was determined by a linear thermal analysis. A concrete thermal conductivity of $\lambda = 2.2 \text{ W m}^{-1} \text{ K}^{-1}$ and a specific heat capacity of $\rho_{cp} = 2.2 \times 10^6 \text{ J m}^{-3} \text{ K}^{-1}$ were considered, while the steel tendons were omitted in the thermal analysis. The temperature evolution reported in Fig. 11 was applied to the internal surface of the representative element of the vessel, while a zero heat flux was im-

posed at the other surfaces. Initially, all the nodes of the model were considered to be at 50 °C. Fig. 10 shows that the heating-cooling cycle applied to the internal surface produces a thermal wave which makes the first meter of material reach considerably temperatures.

4.2. Results and discussion

The results demonstrate that the development of LITS during the fault conditions produces significant stress redistribution in the region close the inner surface. Fig. 11 shows the evolution of both temperature and tension in the vertical tendon *Cable 8*, located at $x=4.00$ m (see Fig. 9), obtained with $\gamma=1.5$, $\gamma=0$ and without LITS in the constitutive model. If LITS is not included in the model, an increase in tension develops on heating, due to the difference in thermal expansion of steel and concrete. This tension is recovered on cooling, due to the perfect recoverability of thermal strain developing in the two materials. By contrast, if LITS is present, a significant drop in tension is obtained in the second part of the heating phase. This is because when the temperature of concrete exceeds the critical temperature $T_{CRIT}=100$ °C, LITS develops and the material relaxes. Such relaxation is not recovered on cooling and produces a drop in tension of 16.80% at the end of the heating-cooling cycle. Moreover, Fig. 11 shows that if LITS is treated as a confinement independent phenomenon ($\gamma=0$), the loss in pre-tension is captured but significantly underestimated. In particular through the traditional approach, only 75% of the drop in prestress predicted through the model proposed here is captured. The results show that the development of LITS is connected to a local loss in precompression in the concrete close to the inner surface of the vessel, therefore representing a potential cause of local material cracking and damage. In the light of this, the inclusion of a LITS model in constitutive laws to be used to perform safety cases of PCPV under accidental heating-cooling cycle appears to be essential. Moreover, these findings demonstrate that the adoption of 3D constitutive models based on the superposition principle may lead to erroneous results.

5. Conclusions

This work presents a novel 3D LITS model to be used for concrete subjected to transient temperatures up to 250 °C. The proposed model captures the experimentally demonstrated dependency of LITS on stress confinement. Here it has been demonstrated using a bilinear uniaxial LITS curve which is conceived to reproduce the general evolution of LITS for different loading conditions. However, the model can be used with any LITS curve that may be appropriate for a given application. The capabilities of the presented LITS model have been demonstrated by verification examples, modeling of experimental tests and an assessment of a typical PCPV under fault conditions.

The following conclusions can be drawn from this study:

- The proposed approach for extending uniaxial LITS curves to 3D captures the dependency of LITS on stress confinement. This dependency is not captured in existing 3D models based on the superposition principle. The confinement factor η introduced here captures this dependency in an intuitive and robust manner.
- Such an approach is flexible. If new tests data for temperatures higher than 250 °C showed that the material sensitivity to the confinement varies with the temperature, the proposed method could still be used by simply defining a temperature-dependent triaxiality scaling factor $\gamma(T)$.
- The proposed bilinear uniaxial model, conceived to be extended to 3D, gives a better approximation of the general trend of the

LITS curves developing for various loading conditions and temperatures up to 250 °C than the existing models, conceived to fit the uniaxial curves.

- LITS plays a key role in the structural behavior of bulk concrete structures subjected to accidental transient heating-cooling. In the case of a PCPV under fault conditions, it was shown that the irrecoverable stress relaxation that takes place in the concrete on heating, results in a significant loss in tension in the prestressing tendons. Such stress redistribution is not captured if LITS is not explicitly modeled. Therefore, it is essential to include LITS in concrete material models to be used in the assessment of such structures in erroneous and possibly dangerous predictions are to be avoided. Furthermore, it has been demonstrated that adopting a simplistic 3D LITS model based on superposition of linear models is also insufficient to make accurate predictions.
- Additional experimental and numerical work is needed for the LITS dependency on the moisture movement to be assessed and modeled.
- The presented LITS model can be theoretically added to any existing concrete constitutive law, including for example damage, plasticity or creep strain components.

Acknowledgments

This work was supported by EPSRC and EDF Energy. The authors wish to thank Dr Mihail Petkovski for the useful discussions.

References

- Anderberg, Y., Thelandersson, S., 1976. Stress and deformation characteristics of concrete at high temperature: 2. experimental investigation and material behavior model. *Bull. No. 46*, Lund 86.
- Anderberg, Y., Thelandersson, S., 1978. A constitutive law for concrete at transient high temperature conditions. *J. Am. Concr. Inst. Spec. Publ.* 55, 187–205. doi:10.14359/6614.
- Bazant, ZP, Raftshol, WJ, 1982. Effect of cracking in drying and shrinkage specimens. *Cem. Concr. Res.* 12, 209–226. doi:10.1016/0008-8846(82)90008-4.
- Bazant, ZP, Chern, JC, 1985. Concrete creep at variable humidity: constitutive law and mechanism. *Mater. Struct.* 18, 1–20. doi:10.1007/BF02473360.
- Bazant, ZP, 1994. Drying creep of concrete: constitutive model and new experiments separating its mechanisms. *Mater. Struct.* 27, 3–14.
- Cohen, MD, Olek, J, Dolch, WL, 1990. Mechanism of plastic shrinkage cracking in portland cement and portland cement-silica fume paste and mortar. *Cem. Concr. Res.* 20, 103–119. doi:10.1016/0008-8846(90)90121-D.
- Colina, H, Sercombe, J, 2004. Transient thermal creep of concrete in service conditions at temperatures up to 300 °C. *Mag. Concr. Res.* 56, 559–574.
- Colina, H, Moreau, G, Cintra, D, 2004. Experimental study of transient thermal creep and other phenomena of concrete at high temperature. *J. Civ. Eng. Manage.* 10, 255–260.
- De Borst, R, Peeters, P, 1989. Analysis of concrete structures under thermal loading. *Comput. Methods Appl. Mech. Eng.* 77, 293–310. doi:10.1016/0045-7825(89)90079-0.
- De Soza T. Code_Aster: guide de lecture de la documentation de référence (<http://www.code-aster.org>) 2013.
- EDF. "Algorithme Non Linéaire Quasi-Statique STAT_NON_LINE." Référence du Code Aster R5.03.01 révision : 10290. (<http://www.code-aster.org>) 2013.
- Ehm, C, Schneider, U, 1985. The high temperature behavior of concrete under biaxial conditions. *Cem. Concr. Res.* 15, 27–34. doi:10.1016/0008-8846(85)90005-5.
- Gawin, D, Pesavento, F, Schrefler, BA, 2004. Modeling of deformations of high strength concrete at elevated temperatures. *Mater. Struct. Constr.* 37, 218–236.
- Gernay, T, Millard, A, Franssen, J-M, 2013. A multi-axial constitutive model for concrete in the fire situation: theoretical formulation. *Int. J. Solids Struct.* 50, 3659–3673. doi:10.1016/j.ijsolstr.2013.07.013.
- Granger, L, 1996. Comportement différé du béton dans les enceintes de centrales nucléaires. Analyse et modélisation - Thèse de doctorat de l'ENPC.
- Gross, H, 1975. High-temperature creep of concrete. *Nucl. Eng. Des.* 32, 129–147. doi:10.1016/0029-5493(75)90095-3.
- Hager, I, 2013. Behavior of cement concrete at high temperature. *Bull. Polish Acad. Sci. Tech. Sci.* 61, 145. doi:10.2478/bpasts-2013-0013.
- Hassen, S, Colina, H, 2006. Transient thermal creep of concrete in accidental conditions at temperatures up to 400 °C. *Mag. Concr. Res.* 58, 201–208. doi:10.1680/macr.2006.58.4.201.
- Helfer, T, Michel, B, Proix, J-M, Salvo, M, Sercombe, J, Casella, M, 2015. Introducing the open-source mfront code generator: application to mechanical behaviors and material knowledge management within the PLEIADES fuel element modeling platform. *Comput. Math Appl.* 70, 994–1023. doi:10.1016/j.camwa.2015.06.027.

- Illston, JM, Sanders, PD, 1973. Effect of temperature change upon the creep of mortar under torsional loading. *Mag. Concr. Res.* 25, 136–144.
- Khennane, A, Baker, G, 1992. Thermoplasticity model for concrete under transient temperature and biaxial stress. *Proc. R. Soc. London A Math Phys. Eng. Sci.* 439, 59–80.
- Khoury, GA, Grainger, BN, Sullivan, PJE, 1985. Transient thermal strain of concrete; literature review, conditions within specimen and behavior of individual constituents. *Mag. Concr. Res.* 37, 131–144.
- Khoury, GA, Grainger, BN, Sullivan, PJE, 1985. Strain of concrete during first heating to 600 °C under load. *Mag. Concr. Res.* 37, 195–215.
- Kordina, K, Ehm, C, Schneider, U, 1986. Effects of biaxial loading on the high temperature behavior of concrete. *Fire Saf. Sci.* 1, 281–290. doi:10.3801/IAFSS.FSS.1-281.
- Law, A, Gillie, M, 2008. Load induced thermal strains: implications for structural behavior. *Fifth International Conference on Structures in Fire.*
- Li, L, Purkiss, J, 2005. Stress-strain constitutive equations of concrete material at elevated temperatures. *Fire Saf. J.* 40, 669–686. doi:10.1016/j.firesaf.2005.06.003.
- Mindeguia, J-C, Hager, I, Pimienta, P, H, Carré, La Borderie, C, 2013. Parametrical study of transient thermal strain of ordinary and high performance concrete. *Cem. Concr. Res.* 48, 40–52.
- Nielsen, CV., Pearce, CJ, Bicanic, N., 2002. Theoretical model of high temperature effects on uniaxial concrete member under elastic restraint. *Mag. Concr. Res.* 54, 239–249. doi:10.1680/mac.54.4.239.38809.
- Parrott, LJ., 1979. Study of transitional thermal creep in hardened cement paste. *Mag. Concr. Res.* 31, 99–103.
- Pearce, CJ, Nielsen, CV, Bićanić, N., 2004. Gradient enhanced thermo-mechanical damage model for concrete at high temperatures including transient thermal creep. *Int. J. Numer. Anal. Methods Geomech.* 28, 715–735. doi:10.1002/nag.376.
- Petkovski, M, Crouch, RS, 2008. Strains under transient hygro-thermal states in concrete loaded in multiaxial compression and heated to 250°C. *Cem. Concr. Res.* 38, 586–596.
- Pickett, G, 1942. The effect of change in moisture-content on the crepe of concrete under a sustained load. *ACI J. Proc.* 38.
- Schneider, U., 1976. Behavior of concrete under thermal steady state and non-steady state conditions. *Fire Mater.* 1, 103–115.
- Schneider, U., 1988. Concrete at high temperatures - a general review. *Fire Saf. J.* 13, 55–68.
- Terro MJ. Numerical modeling of the behavior of concrete structures in fire 1998;95:183–93.
- Thelandersson, S., 1974. Mechanical behavior of concrete under torsional loading at transient, high-temperature conditions. *Bull. No.46* 83.
- Thelandersson, S., 1987. Modeling of combined thermal and mechanical action in concrete. *J. Eng. Mech.* 113, 893–906.
- Thienel, K-C, Rostásy, FS, 1996. Transient creep of concrete under biaxial stress and high temperature. *Cem. Concr. Res.* 26, 1409–1422. doi:10.1016/0008-8846(96)00114-7.
- Torelli, G, Mandal, P, Gillie, M, Tran, V-X., 2016. Concrete strains under transient thermal conditions: a state-of-the-art review. *Eng. Struct.*
- Zienkiewicz, OC., 1977. *The Finite Element Method.* London: McGraw-hill.